LASER INTERFEROMETER GRAVITATIONAL WAVE OBSERVATORY
- LIGO -
CALIFORNIA INSTITUTE OF TECHNOLOGY
MASSACHUSETTS INSTITUTE OF TECHNOLOGY

Engineering Note	**LIGO-E1500247–v1**	2015/10/02

Investigation of Thermal Noise in Thin Silicon Structures

Matthew Winchester
Mentors: Nicolas Smith, Zach Korth, Rana Adhikari

California Institute of Technology
LIGO Project, MS 18-34
Pasadena, CA 91125
Phone (626) 395-2129
Fax (626) 304-9834
E-mail: info@ligo.caltech.edu

Massachusetts Institute of Technology
LIGO Project, Room NW22-295
Cambridge, MA 02139
Phone (617) 253-4824
Fax (617) 253-7014
E-mail: info@ligo.mit.edu

LIGO Hanford Observatory
Route 10, Mile Marker 2
Richland, WA 99352
Phone (509) 372-8106
Fax (509) 372-8137
E-mail: info@ligo.caltech.edu

LIGO Livingston Observatory
19100 LIGO Lane
Livingston, LA 70754
Phone (225) 686-3100
Fax (225) 686-7189
E-mail: info@ligo.caltech.edu

http://www.ligo.caltech.edu/

Contents

Abstract

Current aLIGO (Advanced Laser Interferometer Gravitational-Wave Observatory) suspensions and test masses are built from a fused silica substrate. In an effort to further increase detector sensitivity in the mid LIGO frequency band, which may be limited by thermal noise in the future, cryogenic silicon has become a candidate for the next generation of detector suspensions and test masses due to its excellent mechanical and optical properties. The fluctuation-dissipation theorem links microscopic thermal noise fluctuations with macroscopic material damping, which in turn motivates the study of damping mechanisms in silicon structures. In this project we demonstrate and assess several methods for measuring the quality factor of silicon cantilevers, including a continuous measurement technique capable of measuring the quality factor of several resonant modes simultaneously. We also investigate the effects of parameters such as temperature, cantilever geometry, and surface treatments on the quality factor with the goal of informing future detector suspension designs.

1 Introduction

LIGO (Laser Interferometer Gravitational-Wave Observatory) is a massive physics experiment designed to detect gravitational waves originally predicted by Einstein's general theory of relativity in 1916. Each detector is essentially a Michelson interferometer. As gravitational waves pass through the detectors, they distort local space-time and change the effective path length difference between the two perpendicular arms of the interferometer. This creates a relative phase shift between the two beams and allows for constructive interference at the photodiode detector, resulting in a measureable signal that indicates the presence of gravitational waves. Two independent detectors are operated in Livingston, Louisiana and Hanford, Washington. The second generation of LIGO detectors, Advanced LIGO (aLIGO), have been constructed and are currently being commissioned to optimize sensitivity. The first data run of aLIGO is scheduled to begin in Fall 2015.

Research has already begun concerning the third generation of LIGO detectors. There are many different sources of noise that limit the precision of the experiment, such as shot noise, seismic vibrations, and thermal noise. In the mid frequency band relevant for the detection of gravitational waves ($\sim 10 - 100$Hz), thermal noise in the test masses and suspensions will be a major factor limiting detector sensitivity. The aLIGO test masses and suspensions are made of a fused silica material. Cryogenic silicon is now being considered as an alternative construction material for the next generation of LIGO detectors in order to further reduce thermal noise and increase sensitivity in the low frequency band of interest [1].

Thermal noise can be very difficult to measure directly. However, the fluctuation-dissipation theorem relates the dissipation of a perturbed system to the thermal fluctuations of the system at equilibrium. This means that the mechanical dissipation of the material can be studied instead, and this is usually a much easier approach in practice. Previous work has been done investigating the quality factor of thin silicon flexures through ringdown measurement techniques [2, 3]. This project focuses on both ringdown measurements and more advanced techniques such as continuous measurements using feedback control loops.

2 Driven, Damped Oscillators

An externally driven oscillator with linear damping is most commonly modeled with the differential equation:

$$m\ddot{x} + b\dot{x} + kx = f_{ext} \tag{1}$$

where m is the mass of the oscillator, b is the damping coefficient, and k is the restorative spring constant. This differential equation is easy to solve in the frequency domain by taking the Laplace transform:

$$ms^2X(s) + bsX(s) + kX(s) = F_{ext}(s) \tag{2}$$

The transfer function of the system is defined as the ratio of $X(s)/F_{ext}(s)$:

$$H(s) = \frac{X(s)}{F_{ext}(s)} = \frac{1}{ms^2 + bs + k} \tag{3}$$

The system acts as a second order low pass filter. Our resonators have very small dissipation, so we focus our analysis on the underdamped regime, where $b^2/4km \ll 1$. It is also convenient to introduce the three terms $\gamma = b/m$ (damping ratio), $\omega_0 = \sqrt{k/m}$ (natural frequency), and $\tau = 2/\gamma$ (characteristic time). In this regime, the two poles of the transfer function are at:

$$s = \frac{-\gamma}{2} \pm i\sqrt{\omega_0^2 - \gamma^2/4} \tag{4}$$

The maximum value of $|H(i\omega)|$ is at the frequency $\omega_{max} = \sqrt{\omega_0^2 - \gamma^2/2}$. Taking the same underdamped limit above, the γ^2 term is negligible so $\omega_{max} \approx \omega_0$. A plot of the transfer function with normalized frequency is shown in Figure 1 below, with $\gamma = 0.01$:

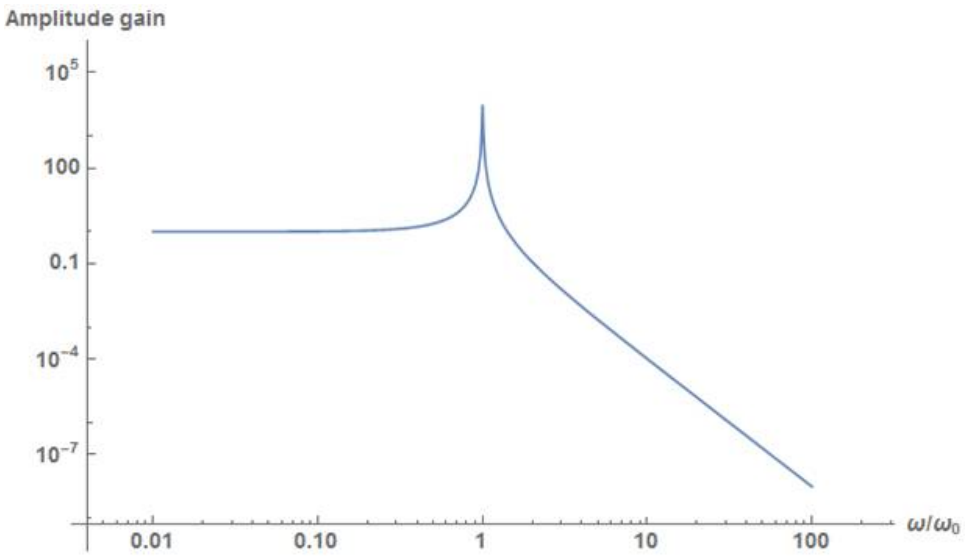

Figure 1: Underdamped Oscillator Transfer Function

The damped oscillator acts as a mechanical second order low-pass filter with a resonance feature around ω_0. The quality factor Q of the resonator is defined as $Q = \omega_0/\Delta$, where Δ

is the full width half max of the transfer function peak. From this definition, we have:

$$Q = \omega_0/\gamma = \frac{\omega_0 \tau}{2} \tag{5}$$

The impulse response of the system can be found by taking the inverse Laplace transform of the transfer function:

$$x(t) = e^{-t/\tau} \sin\left(t\sqrt{\omega_0^2 - \gamma^2/4}\right) \tag{6}$$

where again the γ^2 term can be safely ignored, so the final form of the impulse response is:

$$x(t) = e^{-t/\tau} \sin\left(\omega_0 t\right) \tag{7}$$

An example trace of an underdamped oscillator excited by an impulse is shown below:

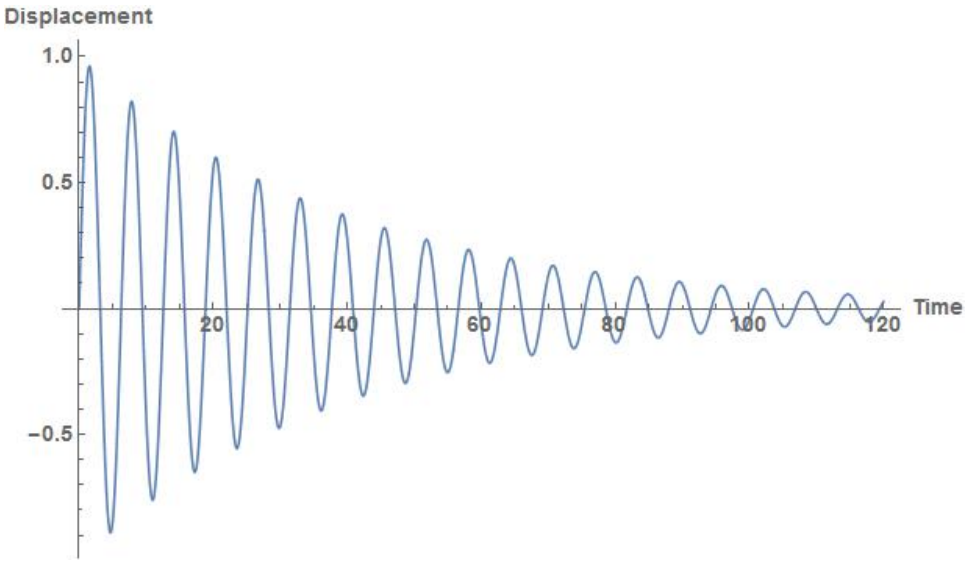

Figure 2: Underdamped Oscillator Impulse Response

3 Internal Damping

Equation 1 is not the only way to model a damped system. Internal damping within materials is frequently described using a complex spring constant k [4]. In this model, the equation of motion becomes:

$$m\ddot{x} + k(1 + i\phi)x = f_{ext} \tag{8}$$

where $\phi(\omega)$ is called the loss angle. The loss angle represents the phase lag between a sinusoidal restorative force and the resulting sinusoidal displacement. It can be shown that the oscillator loses a fraction $2\pi\phi$ of its kinetic energy per cycle by intergrating the work done by the restorative force over a single displacement period. Again taking the Laplace transform and setting the two different parametrizations equal to each other yields the expression:

$$\gamma(\omega) = \frac{\omega_0^2 \phi}{\omega} \tag{9}$$

The quality factor is only defined on resonance $\omega = \omega_0$, so:

$$Q = \frac{1}{\phi(\omega_0)} = \frac{\omega_0 \tau}{2} \tag{10}$$

This relationship forms the motivation for studying the decay time τ of the oscillator. By measuring τ we can calculate the loss ϕ, which then tells us about the thermal noise of the resonator through the fluctuation-dissipation theorem.

4 Fluctuation-dissipation Theorem

Thermal noise is very difficult to measure directly, especially in the extremely low loss mechanical systems used in gravitational wave detectors. However, the fluctuation-dissipation theorem (FDT) relates the dissipation of a perturbed system to the thermal fluctuations of the system at equilibrium [7]. This reversibility symmetry of dissipation was first explored by Einstein with his paper on Brownian motion published in 1905. Brownian motion is the random motion of a larger particle immersed in a fluid of much smaller particles. This motion is the result of many random collisions between the particles. The phenomenon was first noted by the botanist Robert Brown observing the chaotic motion of pollen grains suspended in water. In his paper Einstein proposed the equation:

$$\langle x^2 \rangle = 2Dt \tag{11}$$

where $\langle x^2 \rangle$ is the mean square displacement of the particle, D is the diffusion coefficient and t is the total time that the particle has been free to travel. The diffusion constant is defined as:

$$D = \frac{k_B T}{6\pi\eta r} \tag{12}$$

where k_B is Boltzmann's constant, T is the absolute temperature, η is the fluid viscosity, and r is the particle radius. We can immediately see that this equation relates the thermal fluctuations of a suspended particle, $\langle x^2 \rangle$, to a dissipation mechanism (drag/viscosity). The FDT can also be used to explain phenomena such as Johnson noise in electrical circuits. The mean square voltage measured across a resistor is given by:

$$\langle V^2 \rangle = 4k_B T R \delta v \tag{13}$$

where R is the resistance and δv is the bandwidth over which the voltage is measured. Again we can see the connection between the voltage fluctuations in the resistor and the dissipative resistance. In order to apply the FDT to our damped oscillator system given by equation 8, we define the external force f_{ext} to be a thermal driving force with a spectral density given by:

$$F_{th}^2(\omega) = \frac{4k_B T \phi}{\omega} \tag{14}$$

This results in a noise power spectral density given by:

$$x^2(\omega) = \frac{4k_B T k\phi}{\omega[(k - m\omega^2)^2 + k^2\phi^2]} \tag{15}$$

The equation tells us that (away from resonance) we can decrease the thermal noise in our system by decreasing T and ϕ:

$$\langle x_{th}^2 \rangle \propto \frac{T}{Q} \tag{16}$$

This motivates our study of low loss materials at cryogenic temperatures for potential use in gravitational wave detectors. It is also important to note that equation 16 is only true far away from resonance. In current aLIGO detectors the first violin modes of the suspensions are around 500Hz. From equation 15 it is clear that thermal noise power spectral density is actually directly proportional to Q at resonant frequency ω_0. This is consistent with the equipartition theorem which states that each quadratic term in the systems total energy has a mean value $\frac{1}{2}k_B T$. Changing ϕ alters the distribution of the power spectral density but the integral over all frequencies remains consistent.

5 Experimental Setup

Our lab has two vacuum chambers used for testing silicon resonators. A smaller chamber is used as a prototyping stage where quick testing can be performed on new cantilever designs. The larger chamber is a cryostat used for making measurements at cryogenic temperatures using liquid nitrogen and liquid helium. The cryostat also contains the electronics necessary for making continuous Q measurements.
The silicon cantilever is mounted on one end using a stainless steel clamp and the other end is driven using an electrostatic driver (ESD). Different clamps are used depending on the cantilver geometry. The cantilever displacement is measured by sending a HeNe laser beam through a window in the cryostat. After the beam is reflected off of the cantilever, it returns to a calibrated quadrant photodiode which measures the position of the beam which is proportional to the cantilever displacement. Additional components in the system include a power resistor used to control resonator temperature and a polyether ether ketone (PEEK) base underneath the clamp for insulation from the cold plate. A SolidWorks model of the experimental setup is shown below:

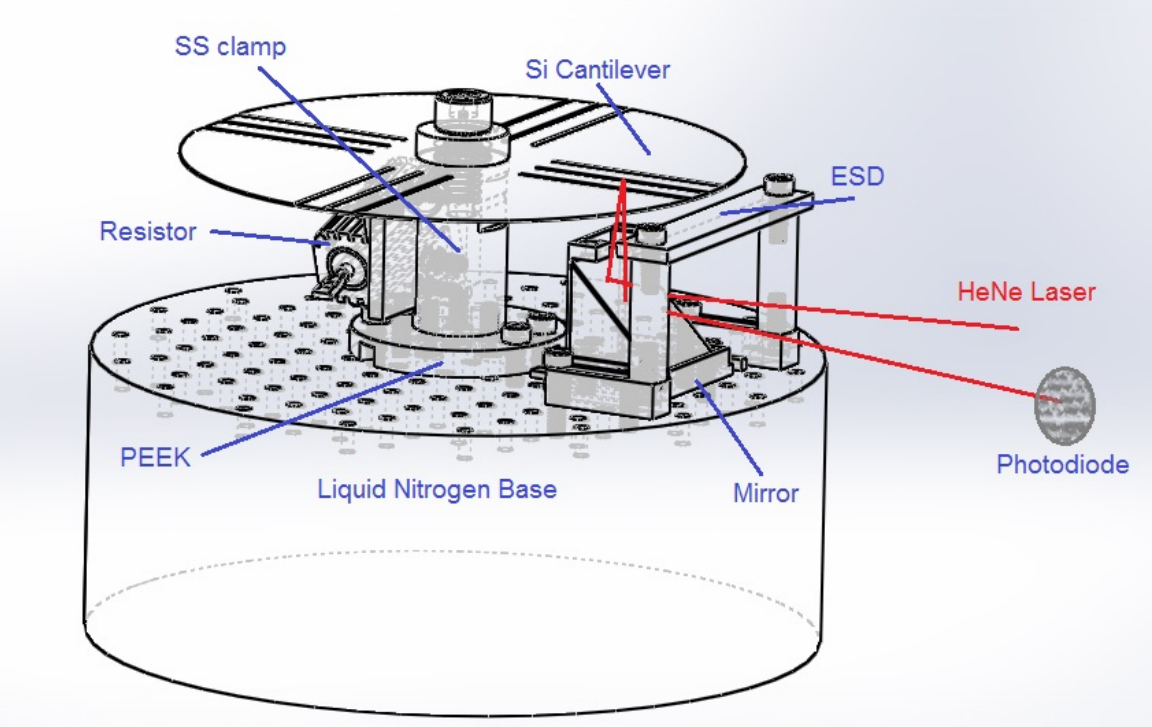

Figure 3: SolidWorks Experiment Model. The silicon cantilever being tested is mounted on a stainless steel post. A laser beam is reflected off the corner mirror onto the cantilever, where it is then reflected back out of the chamber onto a quadrant photodiode The post is attatched to a polyether ether ketone (PEEK) base for insulation necessary to maintain a constant temperature. A power resistor is also fixed to the post in for temperature control. The entire apparatus sits on a liquid nitrogen reservoir.

The following two pictures show the actual clamping setups used to measure both the rectangular and pinwheel shaped cantilevers.

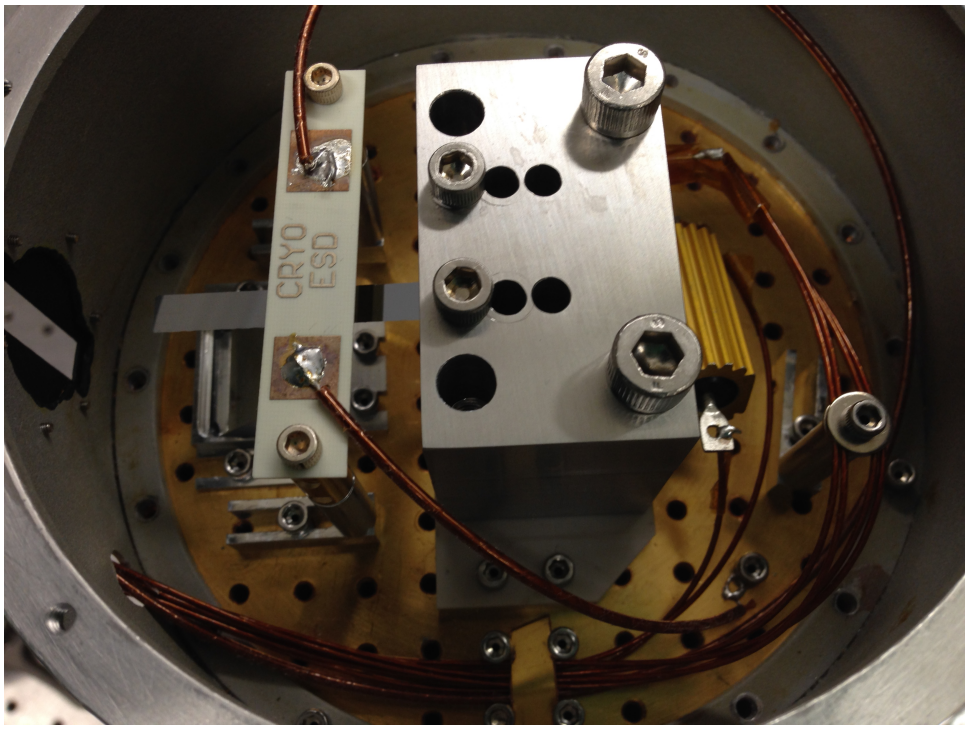

Figure 4: Rectangular Cantilever Mount

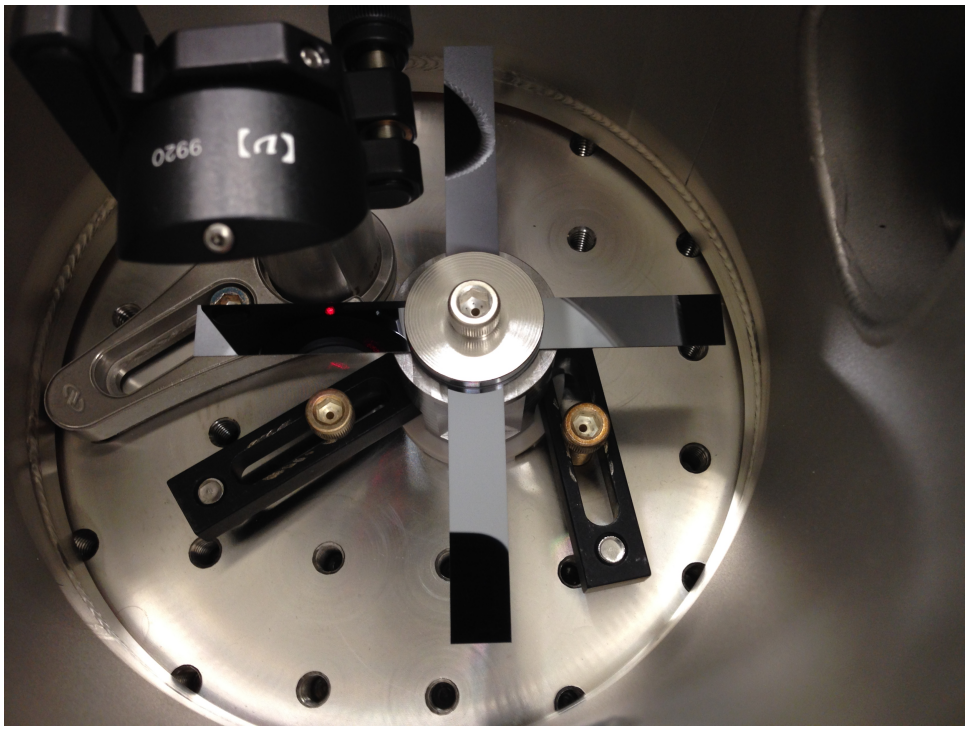

Figure 5: Pinwheel Cantilever Mount

6 Cantilever Designs

We focus our analysis on three silicon cantilever designs. The first is a Glasgow-style cantilever received from a group in Taiwan. Previous measurements indicate that this is the highest quality resonator of the three, most likely due to a combination of better wafer quality and geometry favorable for minimum clamping loss. The dimensions are shown below:

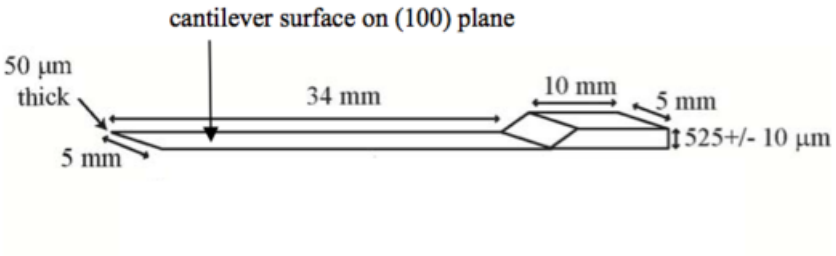

Figure 6: Taiwan Cantilever

We also study a barbell-style cantilever which has a rectangular shape with a thinner section in the middle:

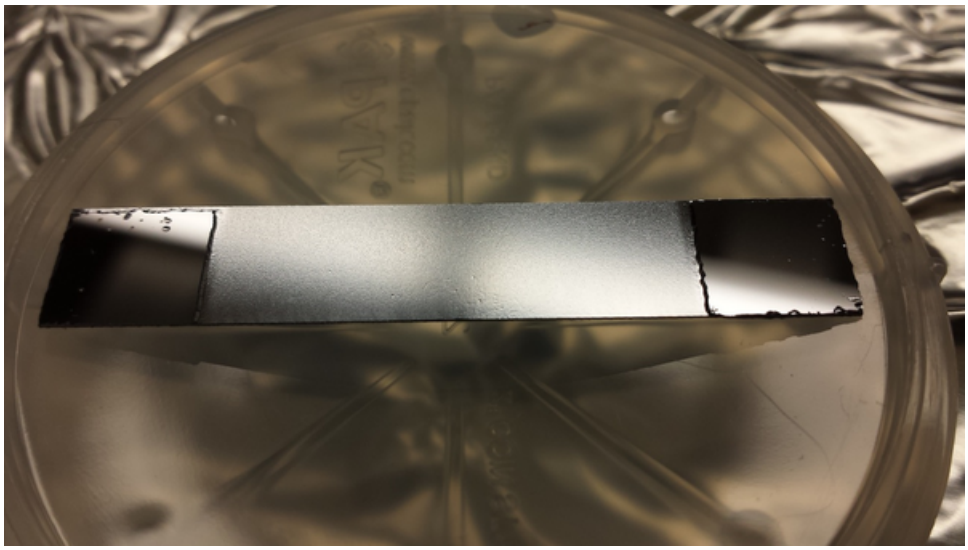

Figure 7: Barbell (Painter2) Cantilever

The entire cantilever is 5cm long and 1cm wide. The two thicker end sections have a thickness of 650μm and the thinner middle section is 250μm thick. The inner section was etched using KOH. Both the Taiwan and Painter2 resonators are mounted in a retectangular clamp.

Lastly we have a pinwheel style resonator that has four cantilever arms of different lengths. This resonator is mounted on a radially symmetric post for measurements. All dimensions shown below are in inches:

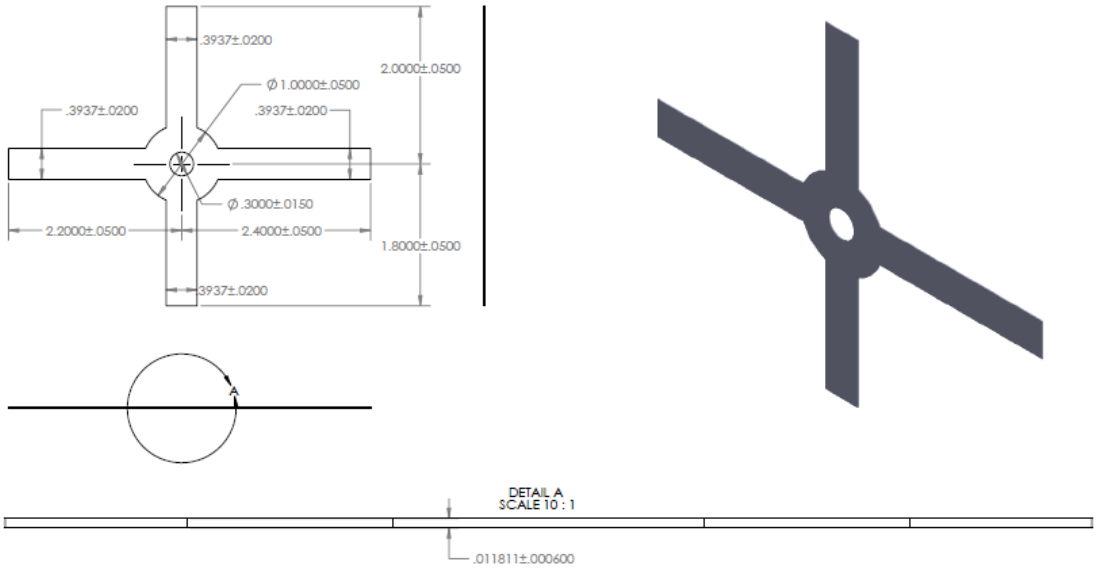

Figure 8: Pinwheel Cantilever

7 Measurement Techniques

7.1 Ringdown Method

In the ringdown experiment we determine the Q factor and loss angle of a thin silicon cantilever by measuring the time constant τ of a damped sinusoidal amplitude signal. We can then use 10 to determine Q. The general data analysis procedure consists of taking a Fourier transform of the amplitude signal and then bandpass filtering around the resonant frequency of the oscillator. An exponential curve can then be fitted to the filtered time domain signal in order to estimate the decay time τ. Several plots outlining this procedure are shown in Figure 9 below:

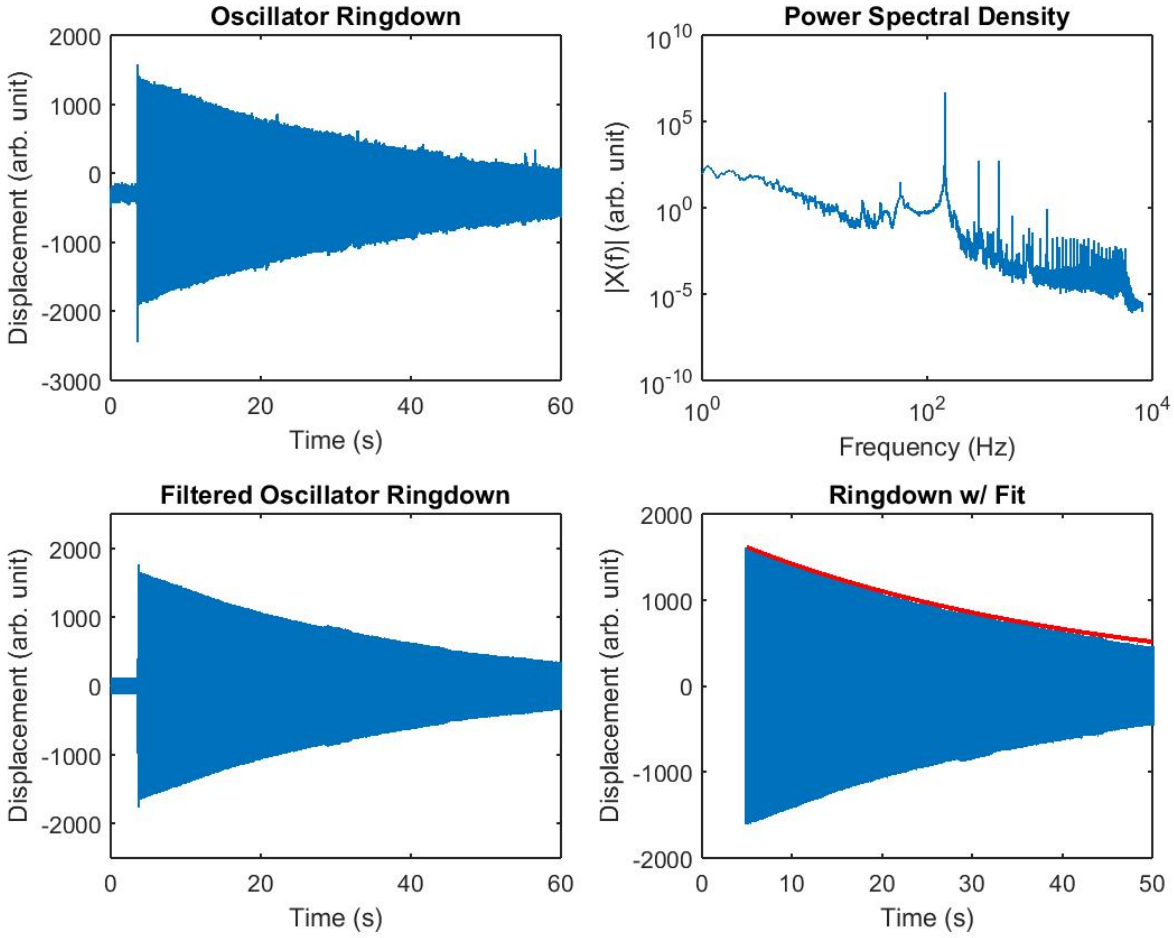

Figure 9: Data Analysis Procedure. Cantilever displacement data is taken from a quadrant photodiode and bandpass filtered around the resonant mode frequency. An exponential curve is then fit to the filtered data in order to estimate the characteristic decay time τ.

In the example analysis above, the Q was determined to be $\approx 17,755$ with $\omega_0/2\pi = 143.9$Hz. This measurement was performed on the fundamental Painter2 cantilever mode at room temperature.

7.2 Continuous Method

In addition to the ringdown method described above, we also utilize a previously developed continuous measurement technique to calculate the Q of our resonators. The continuous measurement technique employs more advanced control systems such as a phase-locked loop (PLL) and amplitude-locked loop (ALL) in order to drive the oscillator under test (OUT) to a constant amplitude. A simple block diagram of the system is shown below:

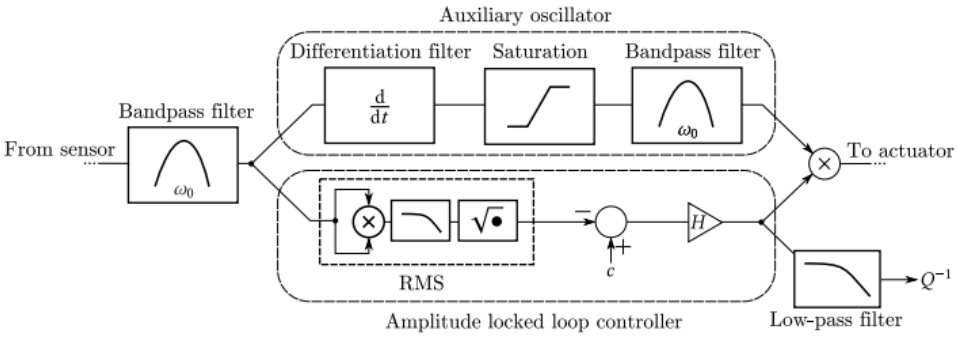

Figure 10: Continuous Measurement Block Diagram

A quadrant photodiode acts as the sensor in our current setup, measuring the relative displacement of the cantilever. From this signal we bandpass filter around the modes resonant frequency ω_0 and send the signal to the ALL and PLL. The PLL first differentiates the signal, producing a 90 degree phase shift. The signal is then amplified and sent through a saturation block where it becomes a square wave. Finally the signal is again bandpass filtered around ω_0 to produce a constant amplitude sine wave phase shifted 90 degrees ahead of the original displacement signal. The ALL works by taking the root mean square of the displacement signal and comparing the result to an amplitude set point c. The resulting error signal is then amplified by gain H and mixed with the PLL output to produce a drive signal for the actuator.
In the limit of high open loop gain where $\omega_U \gg \tau^{-1}$ it can be shown that [6]:

$$\phi = Q^{-1} = \frac{2\omega_U}{cH_U\omega_0}\langle a \rangle \tag{17}$$

Where a is the control output of H, $\omega_U = \frac{|SH_UA|}{2\omega_0}$ is the unity gain frequency (UGF), and H_U is the feedback gain evaluated at the UGF. Angle brackets indicate a time average. The frequency ω_0 can be easily calculated and the remaining parameters can be measured from information required to maintain the control loops.

This measurement technique allows for a continuous measurement of the Q of the resonator, which naturally allows for other parameters such as temperature or amplitude to be swept during the measurement process in order to determine the effect on ϕ. These are important factors when considering clamp design and isolation schemes. It can also be shown that measurements using this technique have a constant signal-to-noise ratio (SNR) since the oscillator is held at a constant amplitude, while the SNR decreases over time with the ringdown method. The continuous method is also useful for measuring very high Q oscillators, where the ringdown decay time may be impractical if not impossible to measure directly.

We have successfully demonstrated the ability to measure different modes simultaneously using this method. However, we are often limited by the actuator gain A due to the physical setup of the experiment. The placement of our actuator, the ESD, heavily influences the modes we are able to excite based on how close the nodes of the particular mode are to the ESD active area. We are also unable to significantly excite torsional modes.

8 Mechanical Losses in Silicon

Mechanical losses in solids come from a variety of different dissipation mechanisms. These include processes such as phonon-phonon loss, surface loss, thermoelastic loss, and bulk loss. We expect thermoelastic loss and surface loss to be significant loss mechanisms due to our silicon resonator geometry. Various other dissipation processes such as gas damping are inevitably present in our system, but should be negligible compared to other losses.

8.1 Thermoelastic Loss

Thermoelastic loss occurs when a solid is bent. As certain local regions are compressed they heat up, while stretched regions are cooled (assuming a positive coefficient of thermal expansion). This creates temperature gradients in the material. Heat fluxes driven by the temperature gradient irreversibley dissipate energy, thus causing loss. Since thermoelastic loss is highly dependent on the material coefficient of thermal expansion, cryogenic silicon naturally becomes a good material choice for high quality mechanical systems due to its vanishing coefficient of thermal expansion at 124K.

For isotropic materials in pure bending modes, the thermoelastic loss ϕ_{TE} is given by the equation [5]:

$$\phi_{TE} = \frac{\alpha^2 Y T}{\rho C_p} \frac{\omega\tau}{1+\omega^2\tau^2} \tag{18}$$

where α is the coefficient of thermal expansion, Y is Young's modulus, T is the temperature, ρ is the material density, C_p is the heat capacity, and ω is the angular frequency of the particular bending mode. The additional time constant τ is defined as:

$$\tau = \frac{\rho C_p t^2}{\pi\kappa} \tag{19}$$

where t is the thickness of the resonator and κ is the thermal conductivity. One of the major reasons that cryogenic silicon is being considered for future gravitational wave detectors is because silicon has a vanishing coefficient of expansion at 124K, so there shouldn't be any thermoelastic loss at this temperature. Figure 11 below shows a plot of the thermoelastic loss ϕ_{TE} as a function of temperature. A thickness $t = 50\mu m$ is assumed:

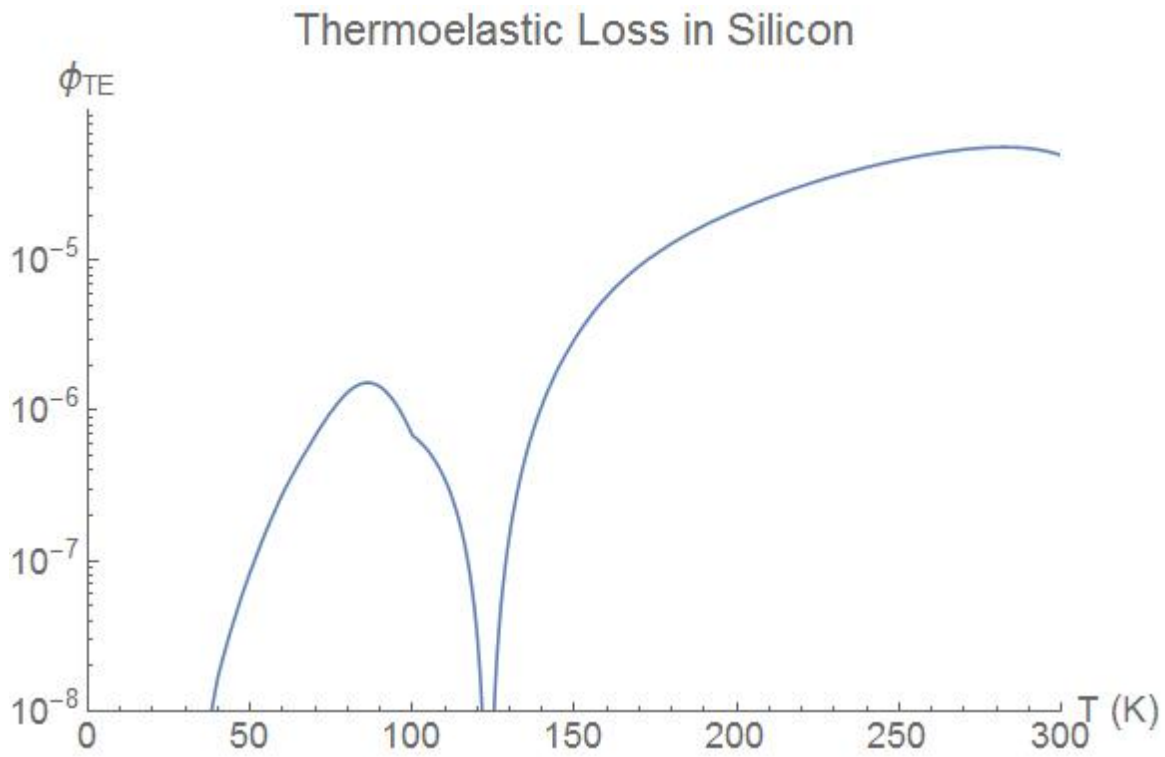

Figure 11: Thermoelastic Loss as a function of temperature. The sharp drop in ϕ at $T =$ 124K corresponds to when α, the thermal expansion coefficient of silicon, goes to zero.

Using 18, we predict a $Q \approx 50,000$ for rectangular cantilevers close to our geometry at room temperature. This value is much higher than both our experimental data and COMSOL FEA modeling which are shown below, indicating that thermoelastic loss probably isn't the limiting factor in our system at room temperature.

Table 1: Thermoelastic Loss in Silicon Pinwheel

Pinwheel Arm Length	Eigenfrequency (Hz)	Q (ringdown method)	COMSOL Predicted Q
2.4″	184	2,260	29,583
2.2″	228	—	23,103
2.0″	294	2,300	17,995
1.8″	392	1,000	12,875

The COMSOL predicted Q is much lower than the theoretical equation because the COMSOL model also considers thermoelastic loss in the clamp and washers. Thermoelastic loss was modeled in COMSOL by simulating temperature gradients caused by streching and squeezing in the cantilever. An example of temperature analysis is shown below using the fundamental mode of the Painter2 cantilever:

(a) Painter2 Cantilever Top

(b) Painter2 Cantilever Bottom

Figure 12: The models above represent relative heating in the cantilever, from which thermoelastic loss is calculated. Red represents warmer, compressed regions while blue represents cooler, stretched regions.

8.2 Clamp Design and Clamp Loss Simulations

We are never truly measuring the cantilever loss in any of our experiments because the cantilever isn't a closed system fixed to an infinitely stiff anchor. Our measured loss is an aggregate of losses in the cantilever, clamp, PEEK base, and even the cyrostat itself. Losses in the clamp have been significant in previous experiments, so optimizing the clamp design to minimize loss is an important task. The ϕ we actually measure can be estimated with the equation:

$$\phi_{measured} \approx \phi_{Si} + \frac{E_{clamp}}{E_{total}}\phi_{clamp} + \frac{E_{PEEK}}{E_{total}}\phi_{PEEK} + ... \tag{20}$$

Where E is the total strain energy stored in the particular component. This formula provides a useful criterion for estimating the merit of new clamp designs.

We designed a completely new clamp for the next series of quality factor measurements. Major changes from the previous model include a much thicker diameter and a lip to constrain the sapphire washers and pinwheel cantilever itself in an effort to decrease clamp loss. The SolidWorks design can be seen below:

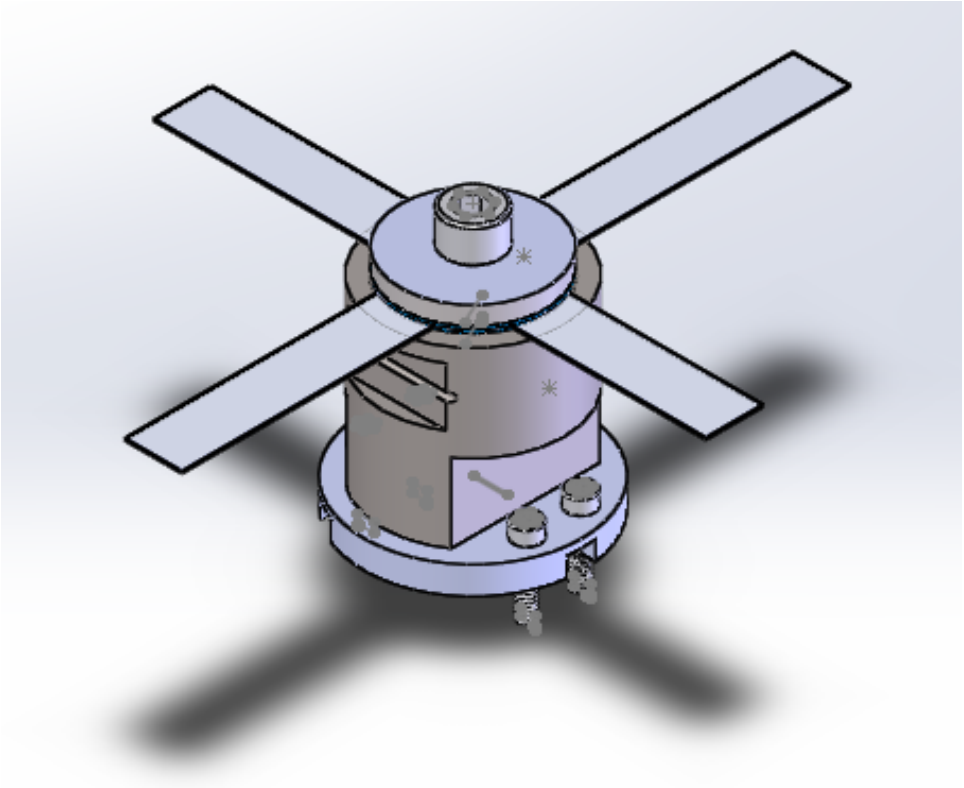

Figure 13: New Clamp Design

In order to test the new clamp design we created a COMSOL model of the system to calculate the strain energy stored in each component for the first several modes of the longest (2.4in) pinwheel cantilever. The model and results are displayed below:

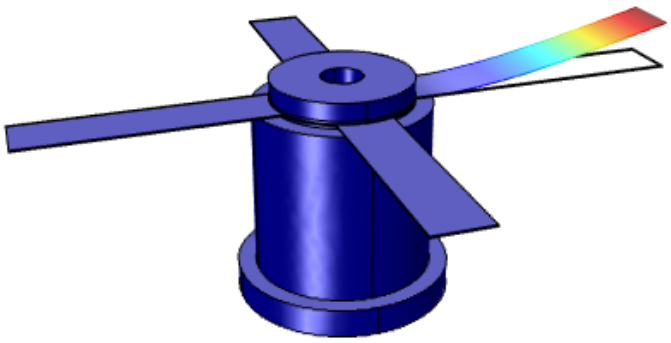

Figure 14: COMSOL Model of 2.4″ Pinwheel Cantilever, Fundamental Mode

Table 2: Elastic Strain Energy Ratio

Eigenfrequency (Hz)	$E_{pinwheel}$ (arb. unit)	E_{clamp} (arb. unit)	Ratio
161	3016	3.4	1.1e-3
1009	120264	139	1.2e-3
1449	212434	160	0.8e-3

The low strain energy ratios indicate that energy leakage into the clamp shouldn't be a significant factor in our measurements.

8.3 Surface Loss

Surface loss effects might also be a significant contribution to the net loss of our resonators. These effects are not well understood and may be influenced by factors like surface roughness, local lattice imperfections, and thin film deposits from other materials. We experimented with surface loss simulations in COMSOL by adding thin, lossy layers to the surface of our cantilever models. The following table shows the computational results of adding 19μm lossy surface layers to the 2.4in pinwheel arm, along with experimental data:

Table 3: Surface Loss in Silicon Pinwheel

Eigenfrequency (Hz)	Q (ringdown method)	Bulk Loss	Surface Loss	COMSOL Predicted Q
161	2,260	2e-5	9e-4	2,230
1009	1,260	1e-4	9e-4	2,044
1449	3,600	8e-6	9e-4	2,280

These simulations closely match our experimental results and may indicate that there is considerable surface loss in our system. With these results in mind, we imaged the surface of the Taiwan cantilever using a USB microscope.

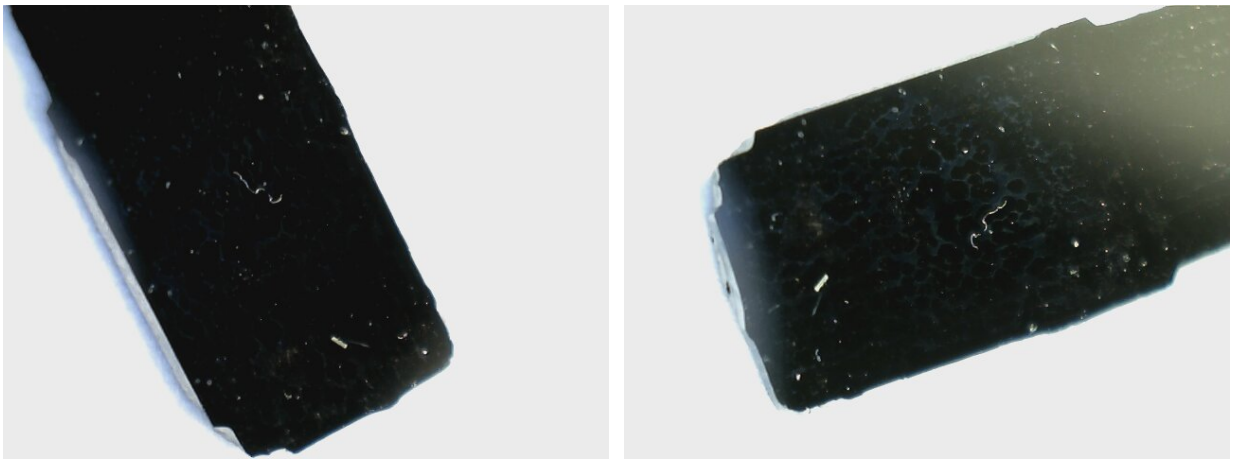

(a) (b)

Figure 15: Taiwan Cantilever Surface

Although it is difficult to make quantitative observations, it is clear that the cantilever surface is not perfectly smooth. In an effort to improve the appearance of the surface, we cleaned the cantilever with isopropyl and again imaged the surface.

(a) (b)

Figure 16: Cleaned Taiwan Cantilever Surface

Large surface imperfections are clearly visible even after the cleaning. While there are no immeadiate remedies for this problem, these results do indicate that we may be limited by lossy surface effects. Surface deformities also appear to grow worse over time since we tend to measure a decreasing Q the more we handle and reclamp the cantilevers. We will continue to explore better manufacturing, etching, and cleaning techniques in order to minimize surface losses.

9 Conclusions

Using a combination of theoretical predictions, computational modeling, and experimentation in the laboratory, we were able to draw several important conclusions from our work. We dont think that thermoelastic or clamp losses are the dominant source of loss in our system. As discussed previously, we dont see a large spike in the quality factor of our resonators around 124K. At this temperature the Q is still two orders of magnitude lower than what we would expect if limited by phonon-phonon losses. Our new clamp design performed similar to the older version despite a significant effort to reduce energy sloshing between the cantilever and mount. There was not a significant change in measured Q from reclamp to reclamp, and these factors indicate that clamp loss wasnt the dominant loss source in our system.

We think that the quality factors of our current cantilevers are limited by surface layer effects. The COMSOL models with thin, lossy surface layers matched experimental data very well. We can also see clear imperfections in the resonator surfaces. This also explains why we tend to measure lower Qs the more we handle the cantilevers.

Aside from looking at different mechanical loss sources in our silicon cantilevers, we also further developed the continuous measurement technique described above. By implementing

multiple instances of the same control loops and filtering around different mode resonances we are able to take continuous measurements of different mode Qs simultaneously. Appropriate filtering can significantly reduce the coupling between modes, and Qs measured with this method agree with results from individual ringdowns and continuous measurements.

10 Future Work

We expect that we are currently limited by surface loss effects. In order to further investigate these phenomena we will begin experimenting with different etching techniques. It will also be important to look at losses in thin films and optical coatings that would be necessary for the test masses in gravitational wave detectors.
A larger cryogenic experiment is also currently under construction. Once the optimal silicon flexure design has been attained, it will be incorporated into the other experiment. The goal of this larger experiment is to directly measure the thermal noise in thin silicon structures by locking a laser to two separate cavities. Each cavity consists of a static mirror and a mirror attached to a silicon structure. Thermal noise can then be measured interferometrically by looking at the beat note formed by the two locked laser beams. The experiment is well into assembly; most optical and electronic systems have been set up.

11 Acknowledgements

The author would like to graciously thank Nicolas Smith, Zach Korth, and Rana Adhikari for their outstanding mentorship and guidance throughout the course of this project. Dmitry Koptsov was also very helpful with COMSOL modeling. This project was supported by the National Science Foundation and the California Institute of Technology through the LIGO SURF program.

List of Figures

List of Tables

References

[1] A.V. Cumming, L. Cunningham, G. D. Hammond, K. Haughian, J. Hough, S. Kroker, I. W. Martin, R. Nawrodt, S. Rowan, C. Schwarz, and A. A. van Veggel, *Silicon mirror suspensions for gravitational wave detectors*. Quantum Grav. 31 025017 (2013).

[2] Edward Taylor, Nicolas Smith, *Quality Factor of Crystalline Silicon at Cryogenic Temperatures*. LIGO Document P1300172-v1 (2013).

[3] Marie Lu, Nicolas Smith, Rana Adhikari, Zach Korth, *Measuring the Quality Factor of Cryogenic Silicon*. LIGO Document T1400668-v1 (2014).

[4] P.R. Saulson, *Thermal Noise in mechanical experiments*. Phys. Rev. D 42, 2437 (1990).

[5] R. Nawrodt, C. Schwarz, S. Kroker, I. W. Martin, F. Brckner, L. Cunningham, V. Groe, A. Grib, D. Heinert, J. Hough, T. Ksebier, E. B. Kley, R. Neubert, S. Reid, S. Rowan, P. Seidel, M. Thrk, A. Tnnermann, *Investigation of mechanical losses of thin silicon flexures at low temperatures*. Quantum Grav. 30, 115008 (2013).

[6] Nicolas Smith, *A technique for continuous measurement of the quality factor of mechanical oscillators*. Review of Scientific Instruments 86, 053907 (2015); doi: 10.1063/1.4920922.

[7] H.B. Callen, T. A. Welton, *Irreversibility and Generalized Noise*. Phys. Rev. 83.1 (1951).